Volume 6
Number 20
21 October 2025
Pages 7129–7620

Materials Advances

rsc.li/materials-advances

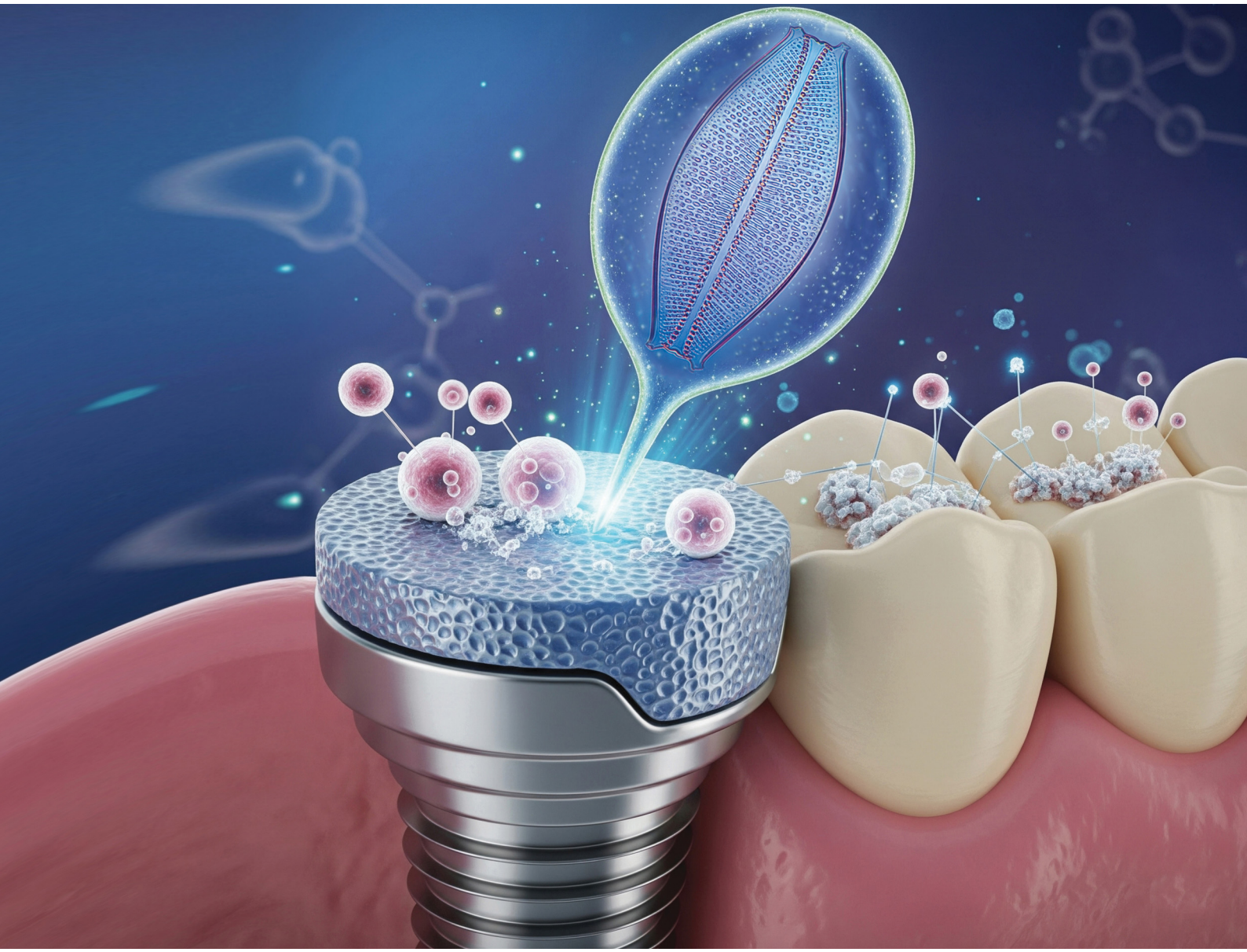

ISSN 2633-5409

ROYAL SOCIETY OF CHEMISTRY

PAPER

Stefania R. Cicco *et al.*
Topographical modification of titanium using diatom biosilica to promote human mesenchymal stem cell proliferation and osteogenic differentiation

Materials Advances

ROYAL SOCIETY OF CHEMISTRY

PAPER

View Article Online
View Journal | View Issue

Cite this: *Mater. Adv.*, 2025, **6**, 7252

Topographical modification of titanium using diatom biosilica to promote human mesenchymal stem cell proliferation and osteogenic differentiation

Rossella Labarile, [a] Danilo Vona, [b] Maria Michela Giangregorio, [c] Roberto Gristina, [c] Vincenza Armenise, [d] Paola Albanese, [e] Gianluca Maria Farinola [d] and Stefania R. Cicco *[f]

Silica-based biomaterials have gained significant attention in the fields of orthopedics and dentistry due to their favorable properties that promote bone regeneration and integration. Techniques such as surface coatings or functionalization can be applied to silica-based biomaterials to further enhance the biological interactions with various composites and hybrid systems, enhancing the properties of polymers, ceramics, and metals used in implants. Diatoms microalgae are fascinating organisms that provide an innovative approach to source silica-based materials sustainably. Diatom-derived biosilica has been proved to be valuable for applications in various fields such as catalysis, drug delivery, environmental remediation. This study explores the potential of *Navicula (N.) pelliculosa*, a benthic diatom, to self-assemble on smooth titanium (Ti) surfaces. This self-adhesion phenomenon and subsequent topographical modification of the titanium surface are exploited to enhance the growth and osteogenic differentiation of hMSCs. By culturing hMSCs on titanium surfaces that have been nanotextured with the hierarchical silica texture of *N. pelliculosa*, increase in calcium deposition is observed within the extracellular matrix, along with elevated collagen production and upregulation of *RUNX2*, *SP7*, and *COL1A1*. These results indicate that the diatom's structure may serve as an effective bioactive interface to facilitate stem cell behavior and promote bone tissue engineering.

Received 22nd May 2025,
Accepted 4th August 2025

DOI: 10.1039/d5ma00525f

rsc.li/materials-advances

1. Introduction

Hybrid biomaterials that significantly enhance bone regeneration are promising candidates for bone grafts and dental implants.[1–3] A critical factor for the success of implants is their ability to achieve osseointegration, which is the integration of the implant with the surrounding bone tissues. Titanium and its alloys are widely preferred for implants due to their exceptional mechanical properties, high resistance to corrosion, and excellent biocompatibility.[4–6]

The improvement of the bioactivity of titanium surfaces can be achieved by topographical, chemical, and biochemical modifications.[7,8] Among these approaches, enhancing bioactivity without the introduction of additional components is particularly beneficial. This simplification minimizes the complexity of the fabrication process, reduces the potential for adverse reactions, and ensures the long-term stability of the modified surfaces. Strategies[9] may include altering the titanium surface morphology to promote cell attachment and proliferation, applying bioactive coatings that release osteogenic factors,[10] or modifying the chemical composition of the surface to enhance interaction with the biological environment.[11] In a pioneer research work, Dalby *et al.* highlighted an innovative approach to directing the differentiation of human mesenchymal stem cells (hMSCs) through nanoscale surface patterns in the absence of osteogenic supplements.[12] The activation of cells derived from a change in surface topography is known as mechano-transduction[13] and involves the conversion of mechanical stimuli into biochemical signals, which can lead to specific chronological genes activation[14] as well as changes in integrins gathering.[15] Differentiation of hMSCs without osteogenic medium can be obtained by texturing

[a] *Consiglio Nazionale delle Ricerche, Istituto per i Processi Chimico-Fisici, via Orabona 4, 70126 Bari, Italy*
[b] *Università degli Studi di Bari A. Moro, Dipartimento di Scienze del Suolo, della Pianta e degli Alimenti, via Orabona 4, 70126 Bari, Italy*
[c] *Consiglio Nazionale delle Ricerche, Istituto per le Nanotecnologie, via Orabona 4, 70126 Bari, Italy*
[d] *Università degli Studi di Bari A. Moro, Dipartimento di Chimica, via Orabona 4, 70126 Bari, Italy*
[e] *Dipartimento di Biotecnologie, Chimica e Farmacia, Università di Siena, via Aldo Moro 2, 53100, Siena, Italy*
[f] *Consiglio Nazionale delle Ricerche, Istituto di Chimica Composti Organometallici, via Orabona 4, 70126, Bari, Italy. E-mail: cicco@ba.iccom.cnr.it*

smooth titanium surfaces[16] using grit blasting before acid etching,[17] chemical surface decoration,[18] plasma etching,[19] sonochemistry,[20,21] and plasma spraying.[22] The challenges associated with traditional biomineralization methods, particularly their environmental impact, scalability, and cost, have led researchers to explore alternative materials for bone tissue engineering.

Mesoporous silica[23] provides effective scaffolding for bone cell growth, attributed to their high mechanical strength, low cytotoxicity, and capacity to enhance both cell proliferation and the osteogenic differentiation of progenitor cells. Furthermore, the unique mesoporous structure enables encapsulation and controlled release of biologically active molecules, which can significantly enhance the therapeutic potential of these scaffolds.[24–27] However, the production of silica-based materials with specific surface topographies involves expensive and labor-intensive methods, which may include the use of toxic alkoxysilanes[28] and harmful solvents.[29] Research efforts are increasingly focused on developing more sustainable and cost-effective manufacturing strategies that can facilitate the widespread application of mesoporous silica in bone tissue engineering while minimizing ecological impact.

Diatoms microalgae are programmed by nature to provide mesoporous silica microparticles known as frustules,[30] with intricate nanotextured surface topography by metabolic biomineralization of *ortho*-silicic acid uptaken from seawater. Diatom frustules naturally feature hierarchically structured silica layers with high porosity, large surface area and tunable pore size depending on the algal species. Furthermore, these silica layers can be easily functionalized through both *in vivo* and *in vitro* methods[31] with a plethora of functional molecules, including organic emitting dyes,[32,33] charged organometallic emitters,[34,35] ions or metal nanoparticles.[36,37]

Surface textured diatomite, made of diatom fossils, ranging in size from 10 to 2000 μm, has been recently utilized to produce bidimensional sintered systems exhibiting cytocompatible features for bone tissue engineering application.[38,39] Even though diatomite is a cheap, abundant and ecological source of silica for bone tissue regeneration, it has drawbacks such as low purity due to mineral contaminations and polydispersity arising from the polymorphic origin of multiple stratified fossil diatoms. Similar systems with monodispersed and pure biosilica extracted from cultured living *Thalassiosira weissflogii* diatoms have been reported by our group to study adhesion, biocompatibility and architectural bio-parameters of bone-related cell types.[40] In our recent work, we demonstrated the production of biosilica-based systems from *T. weissflogii* diatoms that promote fibroblasts and osteoblast-like cells growth and adhesion.[41] Following this investigation, a biosilica-based material *in vivo* doped with sodium alendronate has been studied as osteoinductive promoting bone cells proliferation and anti-erosion phenomenon inhibiting osteoclasts.[42]

In this work, we exploited the unique ability of *Navicula pelliculosa*, a 10–15 μm sized pennate benthic diatom species, to naturally generate biosilica films over smooth titanium surfaces. The resulting nanostructured titanium surfaces were developed with the goal of creating innovative and entirely green scaffolds to promote the osteogenic differentiation of hMSCs.

In vivo decoration of *N. pelliculosa* diatoms with 3-(trimethoxysilyl)propyl methacrylate (MAPTMS) followed by radical photoinitiated polymerization using Irgacure 2959 resulted in the formation of stable, two-dimensional nanotextured titanium-based scaffolds. As a final step, the growth and osteogenic differentiation of hMSCs on the resulting biosilica hybrid scaffolds were thoroughly investigated.

2. Results and discussion

The increased interest in diatoms for biotechnological applications derives from the species-specific variability of frustule morphology together with the tailorable surface chemistry. We selected *N. pelliculosa* diatom due to its natural ability to produce biofilms on flat surfaces and its suitability for *in vivo* functionalization with the MAPTMS monomer, which can subsequently be polymerized using Irgacure 2959 as radical initiator.

2.1. *In-vivo* MAPTMS functionalization

The functionalization with the silane MAPTMS is a widely used technique for modifying surfaces in the biomedical field and in cell culture materials. This silane is particularly effective in enhancing cell adhesion due to its ability to form covalent bonds with surfaces, creating a network of interactions that promote cell attachment. The MAPTMS used as adhesion promoter between titanium and *N. pelliculosa* biosilica was added to the diatoms' culture medium using different feeding approaches (single-step addition *vs*. multi-step addition) testing two concentrations of the monomer (1 or 2 mg mL^{-1}).

In the case of single-step MAPTMS addition, the growth (recorded as number of cells mL^{-1}) of *N. pelliculosa* was negatively affected compared to untreated diatoms regardless of whether the monomer concentration was 1 or 2 mg mL^{-1} (Fig. S1). The growth of the microalgae exhibited a more favorable increasing trend after a 1 mg mL^{-1} MAPTMS multi-step addition compared to a 2 mg mL^{-1} addition. These results suggested that the living microalgae had the ability to grow in MAPTMS supplemented medium. In order to test the stability of diatoms biofilm, solvents and magnetic stirring stress simulation were performed. The biofilm generated by living *N. pelliculosa* cells following 2 mg mL^{-1} MAPTMS multi-step additions was more resistant than biofilm produced after 1 mg mL^{-1} MAPTMS multi-step additions (Fig. S2). The 2 mg mL^{-1} MAPTMS multi-step addition was the optimal feeding method to improve adhesion of *N. pelliculosa* cells on tissue culture polystyrene (TCPS), which was used as test support, although this method resulted in slightly slower cell growth compared to 1 mg mL^{-1} MAPTMS multi-step additions.

After functionalization, Irgacure 2959 was employed as a radical photoinitiator to polymerize MAPTMS, thereby stabilizing the *N. pelliculosa* biofilm on TCPS. The results from Fourier transform infrared spectroscopy in attenuated total reflection

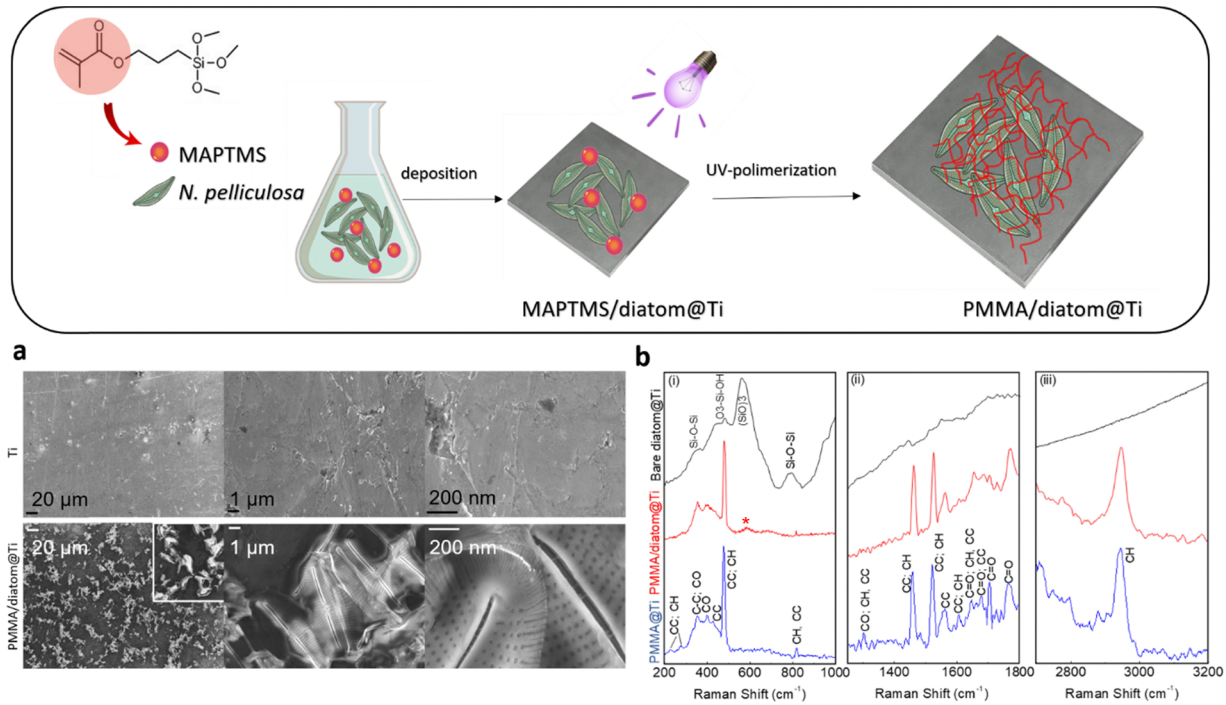

Fig. 1 Schematic representation of the preparation of PMMA/diatom@Ti scaffolds. (a) SEM images of the bare Ti (top) and PMMA/diatom@Ti (bottom) scaffolds. Scale bar: 20 µm, 1 µm and 200 nm. (b) Raman spectra of the bare diatoms (black line), PMMA/diatom@Ti (red line) and PMMA@Ti (blue line) in three different energy ranges (i) 200–1000 cm^{-1}, (ii) 1250–1800 cm^{-1} and (iii) 2700–3200 cm^{-1}. Specific chemical bonds are assigned to vibrational bands. Asterisk (*) indicates the presence of the $(SiO)_3$ bands in the spectrum of PMMA/diatom@Ti.

mode (FTIR-ATR) investigation confirmed MAPTMS upload into frustule nanostructure using the *in vivo* feeding approach (Fig. S3). A characteristic band at 1105 cm^{-1} attributed to Si–O–Si stretching vibrations, associated with the structural backbone of MAPTMS was observed. The signals of the C═O group of acrylate at 1650 cm^{-1} and 1250 cm^{-1}, and methoxy group (–O–CH_3) stretching at 1420 cm^{-1} were recorded when *N. pelliculosa* was functionalized with MAPTMS. A shift at 1650 cm^{-1} and C–H stretching of the aliphatic chain at 2950–2970 cm^{-1} also suggested MAPTMS polymerization of UV-treated samples. The IR spectra confirmed the successful incorporation of MAPTMS into the biosilica matrix, demonstrating that the *in vivo* feeding protocol effectively eliminated the need for harsh and toxic chemical procedures. This approach preserves the stability of the nanostructured biofilm formed by diatom shells on a flat surface using a biocompatible methodology. It provides nanoscale surface patterning to the support while maintaining the integrity of the delicate nanostructure of the diatoms.

2.2. PMMA/diatom@Ti scaffolds production

The same protocol was applied to enable the self-adhesion of *N. pelliculosa* cells on two-dimensional titanium scaffolds. The diatom cells, after being functionalized with MAPTMS according to the described procedure (multi-step addition of 2 mg mL^{-1}), were sedimented onto titanium surfaces for 7 days in order to promote the cells adhesion. Subsequently, the samples were incubated in the dark for 30 minutes with a solution of Irgacure 2959 to initiate the polymerization process and obtain PMMA-embedded diatom cells on titanium (PMMA/diatom@Ti). This step is crucial as it allows the Irgacure 2959 to dissolve and evenly distribute within the medium, ensuring that the subsequent exposure to UV light will trigger the polymerization reaction effectively. Scanning electron microscopy (SEM) images (Fig. 1a) illustrate the surface morphology of PMMA/diatom@Ti at various magnifications. The bare titanium samples displayed a smooth surface with minimal defects, while the PMMA/diatom@Ti samples exhibited a rougher surface texture. This roughness is attributed to the presence of *N. pelliculosa* cells, which retain their architectural integrity. The elliptical valve with rounded ends, split along its longitudinal axis by the raphe, typical features of *Navicula* spp., were clearly recognizable as well as the rectangular sieve plates or puncta (pores and poroids) that collectively form bands of striae between the central ribs and the edge of the valve.

Then, PMMA/diatom@Ti were characterized by Raman spectroscopy (Fig. 1b), and compared to the spectra of the bare diatom and PMMA in three different energy ranges. The Raman spectrum of PMMA on Ti (blue line) showed intense bands due to the presence of C–C, C–H, C–O and C═O bonds in all three energy ranges.[43,44] The identical signals of C–C, C–H, C–O and C═O bands are visible in the Raman spectrum of the PMMA-diatom sample (red line). In addition, the typical diatom feature, *i.e.* $(SiO)_3$-ring breathing mode at ~600 cm^{-1} (indicated by *), confirmed the successful diatom MAPTMS functionalization and subsequent polymerization. The Raman spectrum of the bare diatom, used as control, showed the O–Si–O

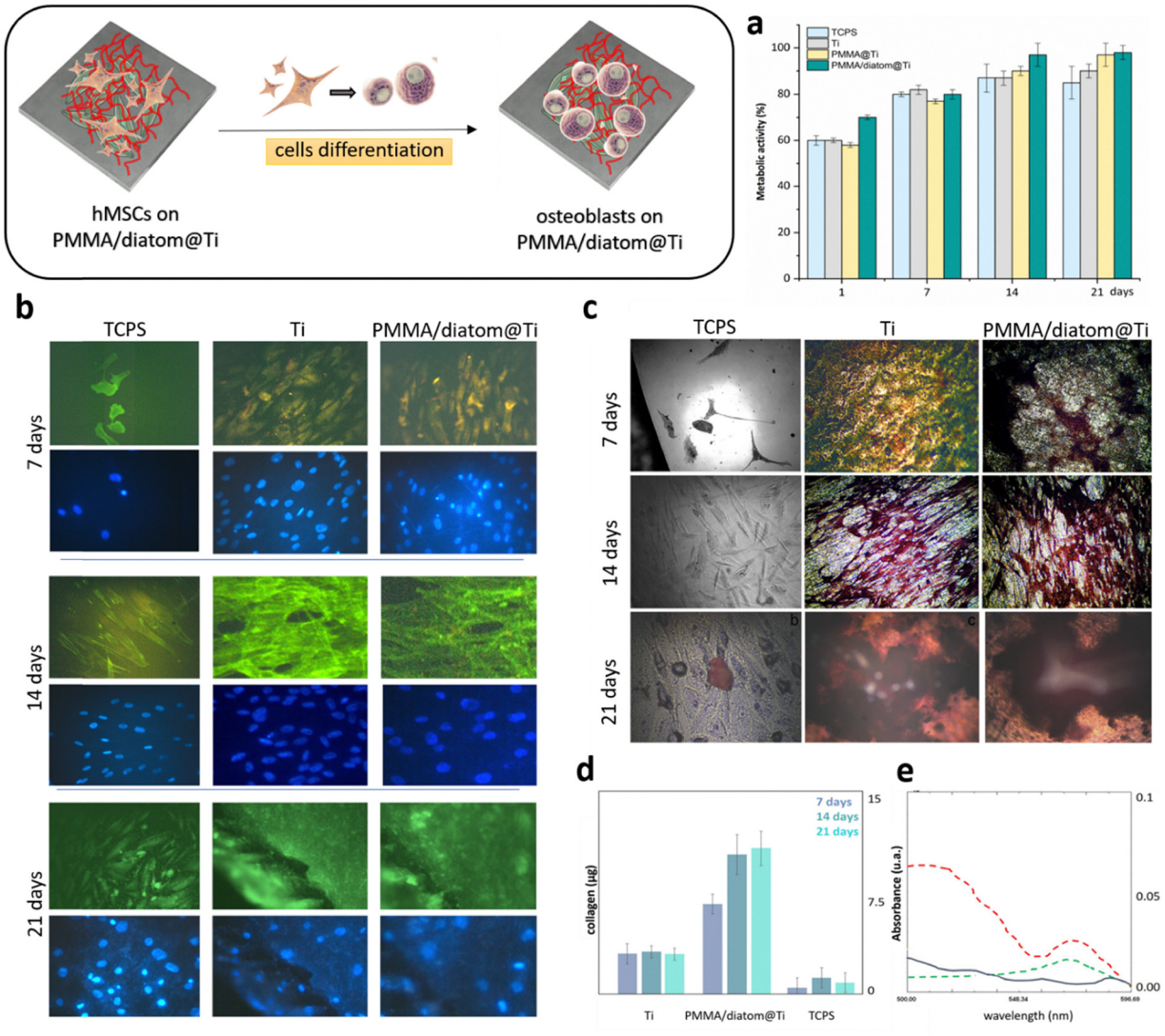

Fig. 2 Biological hMSCs characterization on PMMA/diatom@Ti. (a) Metabolic activity of hMSCs on PMMA/diatom@Ti (green bars) over differentiation time. Tissue culture polystyrene (TCPS, light blue bars), smooth titanium (gray bars) and PMMA@Ti (yellow bars) were used as controls; (b) epifluorescence microscope images (reflection, DAPI/FITC filter cubes) of hMSCs grown on TCPS, smooth Ti and PMMA/diatom@Ti over differentiation time; (c) white light reflection microscopy images of hMSC grown on TCPS, Ti and PMMA/diatom@Ti after Alizarin Red staining over time; (d) mass of collagen (in µg) over days from hMSCs culture on Ti, PMMA/diatom@Ti and TCPS scaffold; (e) absorption spectra of proline signal from smooth Ti (in green), PMMA/diatom@Ti (in red), TCPS (in light gray).

deformation at the wavenumbers below 400 cm^{-1}; the O_3–Si–OH tetragonal vibration at ~500 cm^{-1}, the $(SiO)_3$-ring breathing at ~600 cm^{-1}, and the Si–O–Si symmetric stretching at ~800 cm^{-1}.[45] No significant band shifts are observed in the range 1300–1800 cm^{-1} and 2700–3200 cm^{-1}.

The water contact angle (WCA) measurements indicated that the diatom functionalization significantly increased the hydrophilicity of the titanium surface, as evidenced by the decrease in WCA from 68° for bare Ti to 18° for diatom@Ti and below 10° for PMMA/diatom@Ti. The PMMA coating alone moderately reduced the WCA to 57°, suggesting a less hydrophilic surface compared to the diatom-modified samples.

Regarding surface roughness, the AFM measurements showed that diatom functionalization substantially increased surface roughness (410 nm) compared to bare Ti (106 nm), reflecting the presence of the biosilica structures. The PMMA coating maintained roughness similar to bare Ti, while the combined PMMA/diatom coating preserved a high roughness (~397 nm), indicating that the diatom layer remains exposed or influences the surface topography despite the PMMA overlay (Table S1).

These results demonstrated that diatom functionalization enhances both surface hydrophilicity and roughness, which are important factors influencing cell adhesion and biological interactions, while the PMMA layer modulates these properties depending on its presence and configuration.

2.3. Biological hMSCs characterization on PMMA/diatom@Ti

The protocol proposed for producing PMMA/diatom@Ti scaffolds combines diatoms' self-assembly ability and their natural

3D nanostructure to achieve nanotextured Ti scaffolds to differentiate human mesenchymal stem cells in the absence of osteogenic supplements. Biological analysis of hMSCs were performed seeding the stem cells onto previously described PMMA/diatom@Ti to investigate hMSCs vitality and differentiation process. TCPS, bare Ti and PMMA@Ti were used as controls.

Cellular metabolic activity of hMSCs, expressed by the percentage of Alamar Blue reduction (Fig. 2a), increased steadily throughout the 21-day differentiation period. This upward trend indicates that the PMMA/diatom@Ti scaffold (green bars) does not negatively impact the metabolic activity of hMSCs. Notably, cell viability and proliferation on PMMA/diatom@Ti were more pronounced compared to hMSCs cultured on bare Ti and PMMA@Ti, highlighting its superior biocompatibility over these smoother controls. In contrast, hMSCs cultured on TCPS exhibited a slower metabolic trend.

Epifluorescence microscope images revealed that after 7 days of *in vitro* culture, human mesenchymal stem cells successfully colonized the surface of PMMA/diatom@Ti, adhering to the macroporosity of the microalgae shells. Additionally, the cells formed bridges between the opposite pore walls (Fig. 2b). By days 14 and 21, a uniform layer of cells was observed on the PMMA/diatom@Ti surface, making the supporting scaffold's microarchitecture indistinguishable. As shown, after 14 days of culture, the hMSCs covered the Ti surface and exhibited a fibroblast-like spindle shape that proliferated to form a uniform confluent cell monolayer. The rough nanotextured surface of *N. pelliculosa* embedded in a PMMA matrix served as an effective supportive matrix for cellular growth, enhancing cell adhesion and proliferation over the 21-day period.

Calcium deposition is a crucial indicator of osteogenic differentiation, characterized by the accumulation of calcium salts in the extracellular matrix of hMSCs. This process is vital for bone tissue development and is regulated by a range of biochemical and mechanical signals. The ability of mesenchymal stem cells to deposit calcium presents promising therapeutic opportunities for patients suffering from various tissue defects and injuries. To enhance regenerative treatments, particularly using advanced silica-based biomaterials, scaffolds that create optimal conditions for calcium deposition are essential. The quantification of osteoblast mineralization during osteogenic differentiation is typically assessed using the Alizarin Red S assay, which is recognized as the gold standard in this field.[46] This assay allows for the effective measurement of calcium deposits, providing insights into the osteogenic potential of hMSCs and the efficacy of different scaffold materials in promoting bone formation.

Alizarin Red S staining (Fig. 2c) revealed osteogenic differentiation starting at day 7 in hMSCs cultured on PMMA/diatom@Ti, while it was nearly absent in hMSCs cultured on TCPS. By day 14, the intensity of red staining increased in hMSCs on both Ti and PMMA/diatom@Ti scaffolds, but remained undetectable in the negative control. By day 21, a pronounced Alizarin Red S staining was observed in cells on both Ti-based scaffolds, in contrast to the few red spots seen in hMSCs on TCPS. The staining highlighted the presence of osteon-like structures surrounding the red-stained biomineral deposits on the substrates, suggesting that the cells displayed the characteristic geometrical organization of osteoblasts.

Collagen is a vital component that provides structural support to human mesenchymal stem cells and the surrounding tissue, playing a crucial role in maintaining the mechanical strength and elasticity required for proper tissue function. The presence of collagen in hMSCs is significant for their application in regenerative medicine and tissue engineering, given collagen's essential contribution to the structure and integrity of various tissues.

Using the hydroxyproline assay, we observed that hMSCs cultured on TCPS exhibited almost negligible collagen content at the outset. The collagen levels increased slightly to approximately 3 ± 0.5 μg and remained constant in hMSCs cultured on Ti scaffolds, indicating that the Ti scaffolds did not significantly enhance collagen production in hMSCs during the culture period. The total collagen content increased very rapidly in hMSCs cultured on PMMA/diatom@Ti over differentiation time, from 7.1 ± 1.2 μg after 7 days to 11 ± 3 μg after 21 days (Fig. 2d).

Those data were also supported by absorbance measurement at 550 nm (Fig. 2e). The proline signal is absent for hMSC cultured on TCPS at 14 days, but it was clearly recognizable for hMSC cultured on Ti and was more pronounced for PMMA/diatom@Ti.

The stimulation of collagen production of PMMA/diatom@Ti is particularly advantageous, as collagen is a critical component of the extracellular matrix that supports cell attachment and influences stem cell fate. By promoting the differentiation of hMSCs into osteoblasts, chondrocytes, and adipocytes, this substrate can effectively facilitate the repair and regeneration of various tissues, including bone, cartilage, and adipose tissue.

2.4. Molecular hMSCs characterization

The Runt-related transcription factor 2 (Runx2), encoded by *RUNX2* gene, is the primary and master transcription factor for differentiation of hMSCs into osteoblasts, which further mature into osteocytes. Runx2 is responsive to various stimuli and regulates gene expression through post-translational modifications.[47,48] Runx2 physically interacts and synergistically activates osteogenic genes with another key zinc-finger transcription factor called Osterix/Specificity protein-7 (Sp7), encoded by the *SP7* gene. The Sp7 mRNA expression is predominantly observed in osteoblasts and chondrocytes, and its expression increases during osteoblast maturation from mesenchymal progenitor cells to the pre-osteoblasts and eventually osteocytes.[49,50] Lately, the Sp7 ability to regulate the expression of extracellular matrix proteins such as collagen, bone sialoprotein, osteopontin, fibronectin, and osteocalcin required for mineralization[51] is confirmed by the overexpression of *COL1A1* (Fig. 3). Osteoblasts express high levels of *COL1A1* that encodes a component of type I collagen called the pro-α1(I) chain. This fibril-forming collagen found in most connective tissues is one of the major extracellular matrix proteins produced by osteoblasts. The

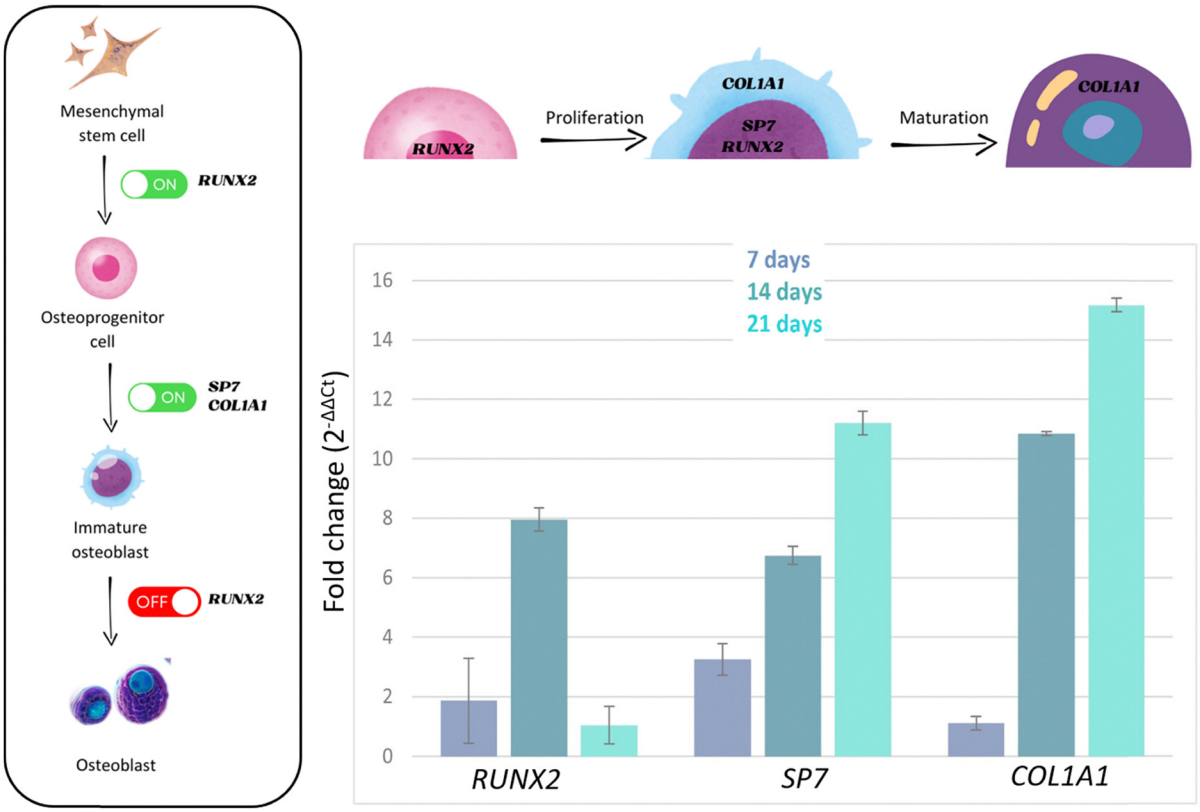

Fig. 3 Osteoblast formation and related genes expression. Fold change of *RUNX2*, *SP7* and *COL1A1* on PMMA/diatom@Ti scaffold after 7 (in gray), 14 (in green) and 21 (in turquoise) days. Error bars represent one standard deviation from the calculated mean for 3 replicates.

combination of two α1 chains and one α2 chain, encoded by *COL1A2* gene, produces the triple-stranded, rope-like procollagen molecules that are processed by enzymes to create very strong mature type I collagen fibers.[52,53]

The mRNA expression of these three candidate markers (*i.e. RUNX2, SP7* and *COL1A1*) for osteoblast differentiation was evaluated to examine the effects of PMMA/diatom@Ti on hMSCs differentiation using quantitative Real Time RT-PCR assay at day 7, 14 and 21. The gene expression levels in hMSC cultured on TCPS for 7, 14 and 21 days were also normalized to *GAPDH* and compared to hMSC cultured on smooth Ti. The expression of the three selected genes in hMSCs cultured on Ti mirrors the trend observed in hMSCs cultured on TCPS over time. Consequently, the hMSCs on Ti were used as a reference control (Fig. S4).

After 7 days, in hMSCs cultured on PMMA/diatom@Ti, *RUNX2* was overexpressed with a 1.8-fold change. The expression peaked at a 7.9-fold increase after 14 days. The expression level returned to a level comparable to hMSCs cultured on Ti after 21 days, suggesting the well-known stabilization of *RUNX2* expression after initial induction (Fig. 3). The *SP7* expression exhibited a 3.2-fold increase after 7 days, while further escalated to an impressive 11.2-fold increase, indicating a sustained positive effect on *SP7* expression over time. The gene *COL1A1* showed a low expression level with only a 0.8-fold change after 7 days. Consistent with the collagen data (Fig. 2d), at day 14 a significant increase was noted with an 11-fold change. After 21 days the *COL1A1* expression reached a 15-fold increase, indicating a strong upregulation of collagen production as the culture progresses. All data were normalized to *GAPDH* and compared with data from hMSCs cultured on Ti.

3. Conclusions

Biosilica-based nanostructured materials represent an innovative technology that will enable advancements in electronics, medicine, energy, and environmental protection, in a future where nanotechnology by bio-inspired materials will play a central role in improving the quality of life and addressing global challenges.

The use of PMMA/diatom@Ti as a substrate for human mesenchymal stem cells presents a promising approach for enhancing cell adhesion, migration, and differentiation. We altered the roughness of the titanium surface by a coating of *N. pelliculosa* embedded in a PMMA matrix that acted as an effective supportive environment for hMSCs adhesion and proliferation over a 21-day period. The cells exhibited a fibroblast-like spindle shape, which is characteristic of healthy growth, allowing them to proliferate and ultimately form a uniform confluent cell monolayer. This result indicates that the nanotextured surface not only supports initial cell attachment but also promotes continued growth and maturation of the cellular layer.

Table 1 Scheme of MAPTMS stock solutions additions in the culture medium at different times

Day	$[MAPTMS]_1$	$[MAPTMS]_2$
0	0.1 mg mL^{-1}	0.13 mg mL^{-1}
2	0.25 mg mL^{-1}	0.33 mg mL^{-1}
4	0.55 mg mL^{-1}	0.73 mg mL^{-1}
7	1 mg mL^{-1}	1.23 mg mL^{-1}
9		2 mg mL^{-1}

Furthermore, the enhanced collagen production observed in hMSCs cultured on PMMA/diatom@Ti underscores the potential of this material that supports and actively guides the differentiation process. Strong evidence of osteoblasts activity provided by staining procedure is supported by the presence of biomineral deposits surrounded by osteon-like structures. Both these characteristics can be strategically utilized in the design of innovative titanium scaffolds tailored for specific tissue engineering applications, ultimately improving the outcomes of regenerative medicine interventions.

The upregulation of osteogenic markers such as *RUNX2*, *SP7* (also known as Osterix), and *COL1A1* provides additional evidence of the osteogenic potential of the hMSCs on the PMMA/diatom@Ti.

Overall, these data indicate that the nanotexturization of titanium substrates using the hierarchical silica texture derived from *N. pelliculosa* significantly promotes the osteogenic differentiation of human mesenchymal stem cells.

The hMSCs osteogenic differentiation promoted by PMMA/diatom@Ti system represents an innovative strategy for bone regeneration and integration in various orthopedic and dental applications. The use of biologically inspired materials as microalgae-based hybrid system may offer a more effective means to support healing and osseointegration, potentially leading to better clinical outcomes in reconstructive surgeries and implants. Further studies could explore the underlying mechanisms driving these enhancements and assess the *in vivo* applicability of this nanotextured surface for bone-related therapies.

4. Experimental

4.1. *In vivo* MAPTMS functionalization

Navicula pelliculosa was cultured in a medium consisting of f/2 Guillard solution enriched with filtered sea water. Cultures were propagated in a vertical bioreactor (18 °C ± 2, 64% relative humidity). The culture medium was further enriched with $Na_2SiO_3 \cdot 9H_2O$. Cold tubes were used as light source with a light/dark cycle set at 12 h light/12 h dark. *N. pelliculosa* cells were grown using the batch (single-step) method in polystyrene flasks dissolving 1 mg mL^{-1} and 2 mg mL^{-1} of MAPTMS (from ethanol stock solutions) into the growth medium. *N. pelliculosa* cells were grown also using multi-step additions of stock solutions of MAPTMS (multi-step) in the culture medium. The scheme of MAPTMS stock solutions additions in the culture medium at different times, is reported in Table 1. Cell density was monitored over 10 days through the use of Burker's hemocytometer. Flasks were manually shaked twice a day to prevent cell adhesion.

Decorated *N. pelliculosa* cells were collected after 10 days by centrifugation at 1500 rpm for 15 min. Pellets were resuspended in f/2 enriched medium after two washes with fresh sea water and seeded in multi-well plates in vertical bioreactor (18 °C ± 2, 64% relative humidity). After 7 days, living diatoms were incubated for 30 min at dark with Irgacure 2959 solution to stabilize the biofilm produced by MAPTMS-fed diatoms. Then wells were washed with bidistilled water and subjected to UV radiation for 45 minutes using a lab UV lamp. Solvent and magnetic stirring stress assays were performed to define the best concentration and the optimal feeding method. MAPTMS-fed diatoms were cleaned adding a solution consisting of 1 g of SDS, 400 μL of methanol, 2% DMSO, 100 mM of EDTA and 20 mL of ddH_2O and left overnight at 75 °C. The extracted diatoms materials underwent a preliminary spectroscopic investigation FTIR-ATR (attenuated total reflection) for analyzing the functional groups present in the samples.

4.2. Production of PMMA/diatom@Ti scaffolds

Titanium (Ti) sheets (1 × 1 cm^2) were activated in a 1 M KOH solution for 20 minutes on a hot plate and rinsed twice with ddH_2O, followed by ethanol washing step. Air-dried Ti sheets were then immersed in a solution consisting of 7 mL of anhydrous hexane and 0.6 mL of diisopropylethylenamine for 5 minutes at room temperature. PMMA@Ti scaffolds were obtained by the addition of 0.5 mL of MAPTMS to the solution and incubation, under stirring, for two hours at 70 °C. After abundant washing in hexane, the PMMA@Ti scaffolds were washed with acetone and ethanol and air-dried, and used as controls.

PMMA/diatom@Ti were assembled using 2 mg mL^{-1} of serial additions of MAPTMS in *N. pelliculosa* growth medium. Irgacure 2959 solution incubation and UV- treatment after 7 days were performed as described before. The extracted diatom materials firmly deposed on Ti sheets underwent spectroscopic investigation *via* Scan Electron Microscopy (SEM) and Raman spectroscopy.

4.3. Static contact angle

The samples wettability was evaluated by static water contact angle (WCA) measurements. These were performed using a Rame – Hart NRL manual goniometer with 1 μL distilled water droplets, at room temperature. Each WCA value represents the average of results obtained from three tests.

4.4. Atomic force microscope (AFM) analysis

For AFM characterization, topographic and phase data were simultaneously acquired using the AutoProbe CP (Thermo-Microscope) microscope using a gold-coated Si tip with a resonant frequency of 80 kHz in non-contact mode.

4.5. Cell culture

Human mesenchymal stem cells (hMSCs, Millipore, Germany) were cultured in DMEM (Microtech, Italy) supplemented with

10% (v/v) FBS, 2 mM L-glutamine and antibiotics (penicillin G sodium 100 U mL^{-1}, streptomycin 100 g mL^{-1}) at 37 °C and 5% CO_2 using polystyrene activated flasks for adherent cells. All the samples for the biological assays were sterilized by soaking them in ethanol and treated under UV. Before each time (7, 14, 21 days), hMSCs were seeded onto the scaffolds starting from a density of 1.6×10^4 cells per sample in multi-well plates.

4.6. Viability assay *via* Alamar Blue test

The Alamar Blue assay (AbD Serotec Ltd., Kidlington, UK) was employed to analyze cell viability. At 7, 14 and 21 days after cell seeding, the different cells-populated scaffolds were rinsed with PBS and DMEM without Phenol Red containing 10% (v/v) Alamar Blue was added for each sample, following the manufacturer's protocol. After 4 h, the optical density at specific wavelengths (570 and 595 nm) were measured. The percentage of Alamar Blue reduction corresponds to viability activity, was evaluated in triplicates and normalized on values of cells grown onto smooth glass.

4.7. Cell morphological analysis

In order to observe the actin cytoskeleton, cells grown on TCPS, Ti and PMMA/diatoms@Ti were fixed and incubated with Alexa Fluor488 phalloidin (Molecular Probes, Eugene, OR, USA).[40] Samples were mounted in Vectashield fluorescent mountant with DAPI (Vector Laboratories, Peterborough, UK) and then observed by means of an epifluorescence microscope (Axiomat, Zeiss, Oberkochen, Germany).

4.8. Alizarin-red staining

To visualize calcium deposition upon osteogenic differentiation, cells-populated scaffolds were pre-treated with PFA (paraformaldehyde) 4% for 20 min, washed 3 times with PBS pH 6.5 (50 mM) and incubated in Alizarin Red staining solution (Sigma) for 45 min. After washing with bidistilled water, samples were observed using an Axiovert 200M (Zeiss) microscope, in reflection mode, acquired with an AxioCam HRC and an AxioVision software.

4.9. Determination of total collagen content

The total collagen content on the surface from three separate wells of each type was quantified using a hydroxyproline assay at 7, 14 and 21 days of osteogenic culture using the previously reported protocol. Briefly the collagen was determined after acid digestion which releases the hydroxyproline, able to form a colored compound with the specific Ehlrich reactant. The color intensity was quantified using the absorbance measurement at 550 nm. The absorbance values were plotted against the hydroxyproline standards and the actual content of hydroxyproline in the experimental samples was extracted from the calibration curve (0–0.1 mg of digested animal collagen). The reactants have been freshly prepared using Chloromine T and Ehrlich reactants as reported in literature. All the samples were collected and hydrolyzed for 2 hours in 1 mL of 6 M HCl at 100 °C; then, after the acid evaporation performed overnight, the samples were rinsed with 1 mL of DI water, evaporated, and a volume of 0.400 mL of chloramine-T solution was added to the hydrolyzates, mixed gently, and the oxidation was allowed to proceed for 25 min at room temperature. Finally, a volume of 0.5 mL of Ehrlich's aldehyde (*p*-dimethylaminobenzaldehyde, DMBA) reagent was added to each sample, mixed gently, and the chromophore was developed by incubating the samples at 65 °C for 20 min. Absorbance of each sample was read at 550 nm using a spectrophotometer.

4.10. RNA isolation, cDNA synthesis and real-time PCR

Total RNA from hMSCs was isolated after 7–14–21 days using Aurum Total RNA Mini Kit (QIAGEN). RNA was dissolved in DEPC ddH_2O and stored at −80 °C until used. For determination of RNA concentration and RNA quality the NanoDrop Spectrophotometer (ND-1000 Spectrophotometer, NanoDrop Technologies Inc.) was employed. cDNAs were synthesized using iScript cDNA Synthesis Kit (Bio-Rad). The cDNAs were subsequently diluted in SsoAdvanced Universal SYBR Green Supermix (Bio-Rad) for the quantitative PCR assay following the manufacturer's instructions. PrimePCR SYBR Green Assay kits (Bio-Rad) of *RUNX2* (qHsaCED0044067), *SP7* (qHsaCED0003759) and *COL1A1* (qHsaCED0043248) were used for the relative gene expression quantification carried out by Real-Time Quantitative PCR. The housekeeping gene glyceraldehydes-3-phosphate dehydrogenase (*GAPDH*, qHsaCED0038674) was used as an endogenous control. The samples were run in triplicate on CFX96 Touch Real-Time PCR Detection System (Bio-Rad) and analyzed by the CFX Maestro software 2.2. The comparative threshold cycle (Ct) method was used to estimate relative changes in gene expressions and fold differences in *RUNX2*, *SP7* and *COL1A1* expression were calculated using the ΔΔCt method, comparing untreated Ti controls to PMMA/diatom@Ti samples and normalizing to *GAPDH*.

Conflicts of interest

There are no conflicts to declare.

Data availability

The data supporting this article have been included as part of the SI.

Supplementary information is available. See DOI: **https://doi.org/10.1039/d5ma00525f**.

Acknowledgements

This work is related to Progetto ''Hub scienze della vita della Regione Puglia'' (codice progetto T4-AN-01 e codice CUP H93C22000560003) Azione 4.1, Piano Operativo Salute, 2014-2020, Ministero della Salute.

References

1 K. M. Percival, V. Paul and G. A. Husseini, *Int. J. Mol. Sci.*, 2024, **25**, 6012.

2 G. Tang, Z. Liu, Y. Liu, J. Yu, X. Wang, Z. Tan and X. Ye, *Front. Cell Dev. Biol.*, 2021, **9**, 665813.
3 M. Yamada and H. Egusa, *J Prosthodont Res.*, 2018, **62**, 152.
4 W. Abd-Elaziem, M. A. Darwish, A. Hamada and W. M. Daoush, *Mater. Des.*, 2024, **241**, 112850.
5 N. Hossain, M. A. Islam, M. M. Shakib Ahmed, M. A. Chowdhury, M. H. Mobarak, M. M. Rahman and M. D. Helal Hossain, *Results Chem.*, 2024, **7**, 101394.
6 E. Marin and A. Lanzutti, *Materials*, 2023, **17**, 114.
7 J. Li, Y. Zheng, Z. Yu, R. K. Kankala, Q. Lin, J. Shi, C. Chen, K. Luo, A. Chen and Q. Zhong, *Heliyon*, 2024, **10**, e23779.
8 P. Yuan, M. Chen, X. Lu, H. Yang, L. Wang, T. Bai, W. Zhou, T. Liu and S. Yu, *J. Mater. Chem. B*, 2024, **12**, 10516.
9 S. Tuikampee, P. Chaijareenont, P. Rungsiyakull and A. Yavirach, *Metals*, 2024, **14**, 515.
10 X. Lu, Z. Wu, K. Xu, X. Wang, S. Wang, H. Qiu, X. Li and J. Chen, *Front. Bioeng. Biotechnol.*, 2021, **9**, 783816.
11 P. Jiang, Y. Zhang, R. Hu, B. Shi, L. Zhang, Q. Huang, Y. Yang, P. Tang and C. Lin, *Bioact. Mater.*, 2023, **27**, 15.
12 M. J. Dalby, N. Gadegaard, R. Tare, A. Andar, M. O. Riehle, P. Herzyk, C. D. Wilkinson and R. O. Oreffo, *Nat. Mater.*, 2007, **6**, 997.
13 J. Mitra, G. Tripathi, A. Sharma and B. Basu, *RSC Adv.*, 2013, **3**, 11073.
14 M. J. Dalby, M. J. Biggs, N. Gadegaard, G. Kalna, C. D. Wilkinson and A. S. Curtis, *J. Cell. Biochem.*, 2007, **100**, 326.
15 V. Petit and J. P. Thiery, *Biol. Cell.*, 2000, **92**, 477.
16 A. Jemat, M. J. Ghazali, M. Razali and Y. Otsuka, *BioMed Res. Int.*, 2015, 791725.
17 W. Chen, Y. Shao, X. Li, G. Zhao and J. Fu, *Nano Today*, 2014, **9**, 759.
18 D. S. Benoit, M. P. Schwartz, A. R. Durney and K. S. Anseth, *Nat. Mater.*, 2008, **7**, 816.
19 S. A. Ulasevich, A. I. Kulak, S. K. Poznyak, S. A. Karpushenkov, A. D. Lisenkov and E. V. Skorb, *RSC Adv.*, 2016, **6**, 62540.
20 E. Kuvyrkov, N. Brezhneva, S. A. Ulasevich and E. V. Skorb, *Ultrason. Sonochem.*, 2019, **52**, 437.
21 Y. U. Kuvyrkou, N. Brezhneva, E. V. Skorb and S. A. Ulasevich, *RSC Adv.*, 2021, **11**, 3843.
22 V. Koshuro, E. Osipova, O. Markelova, M. Fomina, A. Zakharevich, S. Pichkhidze and A. Fomin, *Ceram. Int.*, 2023, **49**, 2034.
23 S. Wang, X. Wang, F. G. Draenert, O. Albert, H. C. Schroder, V. Mailander, G. Mitov and W. E. Muller, *Bone*, 2014, **67**, 292.
24 R. Eivazzadeh-Keihan, K. K. Chenab, R. Taheri-Ledari, J. Mosafer, S. M. Hashemi, A. Mokhtarzadeh, A. Maleki and M. R. Hamblin, *Mater. Sci. Eng., C*, 2020, **107**, 110267.
25 S. Ghosh and T. J. Webster, *Front. Mater.*, 2021, **8**, 692309.
26 J. Wang, B. Du, Z. Fan, S. Li, P. Yun and F. Su, *Polym. Adv. Technol.*, 2018, **29**, 1322.
27 Y. Xu, D. Gao, P. Feng, C. Gao, S. Peng, H. Ma, S. Yang and C. Shuai, *Appl. Surf. Sci.*, 2017, **423**, 314.
28 J. P. Matinlinna, C. Y. K. Lung and J. K. H. Tsoi, *Dent. Mater.*, 2018, **34**, 13.
29 I. A. Rahman and V. Padavettan, *J. Nanomater.*, 2012, 1.
30 R. Gordon, D. Losic, M. A. Tiffany, S. S. Nagy and F. A. Sterrenburg, *Trends Biotechnol.*, 2009, **27**, 116.
31 R. Ragni, S. R. Cicco, D. Vona and G. M. Farinola, *Adv. Mater.*, 2018, **30**, e1704289.
32 G. Leone, G. De la Cruz Valbuena, S. R. Cicco, D. Vona, E. Altamura, R. Ragni, E. Molotokaite, M. Cecchin, S. Cazzaniga, M. Ballottari, C. D'Andrea, G. Lanzani and G. M. Farinola, *Sci. Rep.*, 2021, **11**, 5209.
33 R. Ragni, F. Scotognella, D. Vona, L. Moretti, E. Altamura, G. Ceccone, D. Mehn, S. R. Cicco, F. Palumbo, G. Lanzani and G. M. Farinola, *Adv. Funct. Mater.*, 2018, **28**, 1706214.
34 G. Della Rosa, D. Vona, A. Aloisi, R. Ragni, R. Di Corato, M. Lo Presti, S. R. Cicco, E. Altamura, A. Taurino, M. Catalano, G. M. Farinola and R. Rinaldi, *ACS Sustainable Chem. Eng.*, 2018, **7**, 2207.
35 D. Vona, R. Ragni, E. Altamura, P. Albanese, M. M. Giangregorio, S. R. Cicco and G. M. Farinola, *Appl. Sci.*, 2021, **11**, 3327.
36 G. Leone, D. Vona, M. Lo Presti, L. Urbano, S. Cicco, R. Gristina, F. Palumbo, R. Ragni and G. M. Farinola, *MRS Adv.*, 2017, **2**, 1047.
37 D. Vona Cicco, S. R. Ragni, R. Vicente-Garcia, C. Leone, G. Giangregorio, M. M. Palumbo, F. Altamura and E. Farinola, *Photochem. Photobiol. Sci.*, 2022, **21**, 949.
38 S. R. Cicco, D. Vona, G. Leone, M. Lo Presti, F. Palumbo, E. Altamura, R. Ragni and G. M. Farinola, *MRS Commun.*, 2017, **7**, 214.
39 A. D. Dalgic, D. Atila, A. Karatas, A. Tezcaner and D. Keskin, *Mater. Sci. Eng., C*, 2019, **100**, 735.
40 S. R. Cicco, D. Vona, R. Gristina, E. Sardella, R. Ragni, M. Lo Presti and G. M. Farinola, *Bioengineering*, 2016, **3**, 35.
41 S. R. Cicco, D. Vona, E. De Giglio, S. Cometa, M. Mattioli-Belmonte, F. Palumbo, R. Ragni and G. M. Farinola, *ChemPlusChem*, 2015, **80**, 1104.
42 S. R. Cicco, D. Vona, G. Leone, E. De Giglio, M. A. Bonifacio, S. Cometa, S. Fiore, F. Palumbo, R. Ragni and G. M. Farinola, *Mater. Sci. Eng., C*, 2019, **104**, 109897.
43 I. Kostova, N. Peica and W. Kiefer, *J. Raman Spectrosc.*, 2006, **38**, 1.
44 A. Espina, S. Sanchez-Cortes and Z. Jurasekova, *Molecules*, 2022, **27**, 279.
45 P. Yuan, H. P. He, D. Q. Wu, D. Q. Wang and L. J. Chen, *Spectrochim. Acta, Part A*, 2004, **60**, 2941.
46 A. Bernar, J. V. Gebetsberger, M. Bauer, W. Streif and M. Schirmer, *Int. J. Mol. Sci.*, 2022, **24**, 723.
47 M. Bruderer, R. G. Richards, M. Alini and M. J. Stoddart, *Eur. Cell Mater.*, 2014, **28**, 269.
48 L. Thiagarajan, H. A. M. Abu-Awwad and J. E. Dixon, *Stem Cells Transl. Med.*, 2017, **6**, 2146.
49 K. Nakashima and B. de Crombrugghe, *Trends Genet.*, 2003, **19**, 458.
50 H. Rashid, C. Ma, H. Chen, H. Wang, M. Q. Hassan, K. Sinha, B. de Crombrugghe and A. Javed, *Connect. Tissue Res.*, 2014, **55**(1), 83.
51 M. Milona, J. E. Gough and A. J. Edgar, *BMC Genomics*, 2003, **4**, 43.
52 Y. Zhang and B. Stefanovic, *Int. J. Mol. Sci.*, 2016, **17**, 419.
53 L. Song, N. E. Webb, Y. Song and R. S. Tuan, *Stem Cells*, 2006, **24**, 1707.